Supporting Information

for

Deep reconstruction of Mo-based electrocatalyst for high-performance water/seawater oxidation at ampere-level current density

Jianpeng Sun[a,b], Shuai Zhou[b,c], Zhan Zhao[a], Shiyu Qin[a], Xiangchao Meng[a], Chen-Ho Tung[b,c] and Li-Zhu Wu[b,c*]*

[a]Key Laboratory of Marine Chemistry Theory and Technology (Ministry of Education), College of Chemistry & Chemical Engineering, Ocean University of China, Qingdao, Shandong, 266100, China.

[b]Key Laboratory of Photochemical Conversion and Optoelectronic Materials, New Cornerstone Science Laboratory, Technical Institute of Physics and Chemistry, Chinese Academy of Science, Beijing, 100190, China

[c]School of Future Technology, University of Chinese Academy of Sciences, Beijing, 100049, China

Experimental section

Preparation of $FeMoO_2$/NF

$FeMoO_2$/NF was synthesised by a method similar to that of MoO_2/NF, except that the addition of 100 mg of $Fe(NO_3)_3 \cdot 9H_2O$ to the precursor synthesis.

Preparation of s-FeMoOOH/NF

A typical three-electrode system were used to prepare s-FeMoOOH/NF. Among them, a carbon counter electrode and a SCE were used as the counter electrode and the reference electrode. And then, $FeMoO_2$/NF was placed in 1.0 M KOH solution as the working electrode. Subsequently, electrochemical anodic reconstruction was performed at a constant voltage (0.87 V *vs.* Hg/HgO) of 2 h to obtain the surface amorphous s-FeMoOOH/NF electrocatalysts.

Electrochemical measurements

The OER activity of samples were tested in CHI 660E electrochemical workstation with a typical three-electrode system. The counter electrode and the reference electrode were Graphite rod and a Hg/HgO electrode, respectively. The equation ($E_{RHE} = E_{Hg/HgO} + 0.0592pH + 0.098\ V$) was applied to the conversion of the applied potentials. LSV curves were performed at a scan rate of 5 mV s^{-1} with 100% iR-compensation. The electrochemically active surface areas (ECSA) were calculated from the CV curves at various scan rates. The electrochemical impedance spectroscopy (EIS) were obtained with frequencies ranging from 10^5 Hz to 10^{-2} Hz at 10 mA cm^{-2}. The stability tests were conducted under a constant voltage. Alkaline seawater was collected by dissolving 28 g of potassium hydroxide in natural seawater in a 500-mL volumetric bottle. During the measurement, high-purity O_2 has been bubbled through the electrolyte to saturate it and fix the reversible oxygen potential. The dimensions of the FeMoOOH/NF electrodes were 0.25 cm^2. The anion-exchange membrane (FAA-3–50) was purchased from Suzhou Sinero Technology Co., Ltd.

The Proton Reaction Order (ρ^{RHE}) represented the dependence of OER reaction kinetics on proton activity and was defined by the following formula:

$$\rho^{RHE} = \partial \log(j)/\partial pH$$

In this case, the pH value had ranged from 12.5 to 13.5, and log(j) referred to the logarithm of the current density at 1.5 V versus RHE. When proton-coupled electron transfer reactions occurred, the OER kinetics were nearly independent of the pH value of the solution, resulting in a low ρRHE. On the other hand, if non-synergistic proton-electron transfer was involved in the OER, the kinetics would display a strong pH-dependence, leading to a higher ρ^{RHE} value.

Regarding the ^{18}O isotope labeling experiments, both FeMoOOH/NF and MoO_x/NF had first been activated by the electrochemical CV method (ranging from 0 to 1.8 V versus Hg/HgO, across 10 CV cycles) in an ^{18}O-labeled KOH electrolyte. They then underwent an OER test (20 mA cm^{-2} for 10 minutes) in 1.0 M KOH using regular H_2O. Following this, the gas was collected for GC-MS analysis.

The efficiency of electro-hydrogen energy conversion (η_{ETH}) and the electricity consumption per cubic meter of hydrogen (E_{H2}, kW h Nm^{-3}) were calculated using the unit electric quantity per cubic meter of hydrogen (Q_u, A h Nm^{-3}) and cell voltage (V, V) at an industrially relevant current density of 500 mA cm^{-2}, as follows:

$$Q_u = \frac{2N_A e}{3600 \times 22.43 \times 10^{-3}} = 2390\ A\ h\ Nm^{-3}$$

where 1.48 V represents the thermal-neutral voltage for overall water splitting, and e and N_A denote the electron charge and Avogadro's number (6.022×10^{23} mol^{-1}), respectively.

For the $Co_2Mo_3O_8$/MoO_2/NF//FeMoOOH/NF electrolyzer,

$$E_{H2} = \frac{Q_u V}{1000} = 2390 \times 1.64 \div 1000 = 3.94\ km\ h\ Nm^{-3}$$

$$\eta_{ETH} = \frac{1.48 \times Q_u}{E_{H2} \times 1000} \times 100\% = \frac{1.48 \times 2390}{3.94 \times 1000} \times 100\% = 89.7\%$$

DFT computations:

Theoretical calculations were performed via the Vienna ab initio software package (VASP). The computational procedure employed the gradient approximation (GGA) with the Perdew-Burke-Ernzerhof (PBE) parameterization was used to represent the exchange-correlation energies. The phase structure was modeled using a 3 × 3 × 1 k-point mesh in the Brillouin zone. Computational parameters included an energy cutoff of 300 eV, and convergence thresholds for force and energy were set to 0.05 $eV \cdot Å^{-1}$ and 10^{-5} eV, respectively. The vacuum layer was 15 Å.

Characterization:

X-ray diffraction (XRD) was tested on the Bruker D8 focus. Hitachi S-4800 and JEOL JEM 2100 were used to study scanning electron microscope (SEM) and high-resolution transmission electron microscopy (HRTEM), respectively. The energy dispersive X-ray (EDX) element mapping images were studied on the TEM equipped. The X-ray photoelectron spectroscopy (XPS) spectra were tested on ESCALAB 250Xi. The in-suit Raman tests were performed on Renishaw inVia-Qontor using a 532 nm laser excitation. The inductively coupled plasma-mass spectrometry (ICP-MS) were evaluated by Varian 710-OES. In-situ attenuated total reflection infrared (ATR-IR) spectra was performed between 1.2 V to 1.7 V *vs.* RHE.

Figures

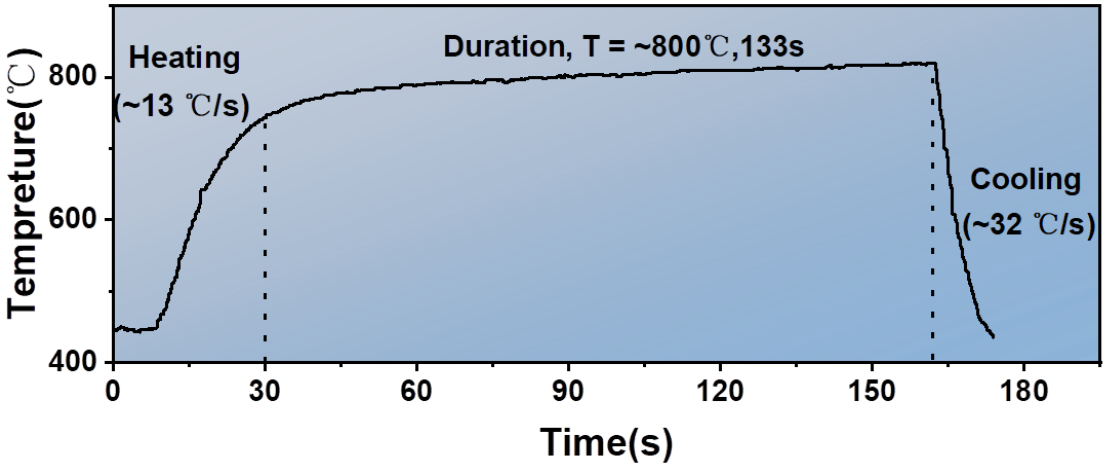

Fig. S1. Real time reaction temperature of carbothermal shocking process of MoO_2/NF.

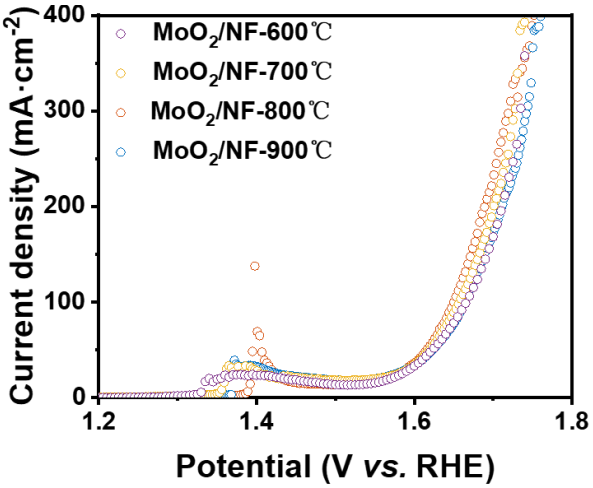

Fig. S2. (b) OER polarization curves of MoO_2/NF at different temperatures.

Fig. S3. The schematic representation of anodic reconstruction.

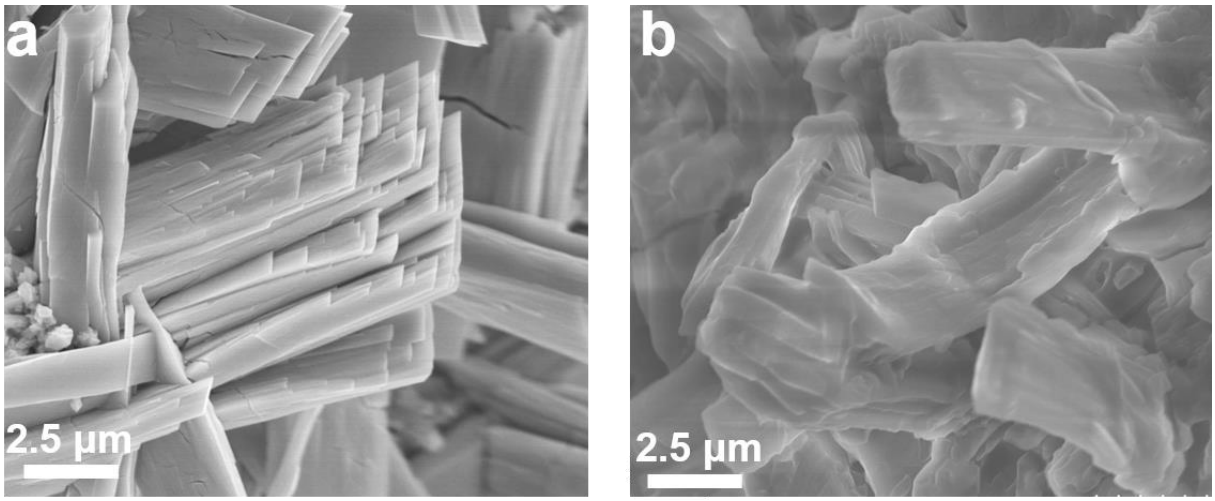

Fig. S4. SEM of (a) FeMoOOH/NF-0 h and (b) FeMoOOH/NF-2 h.

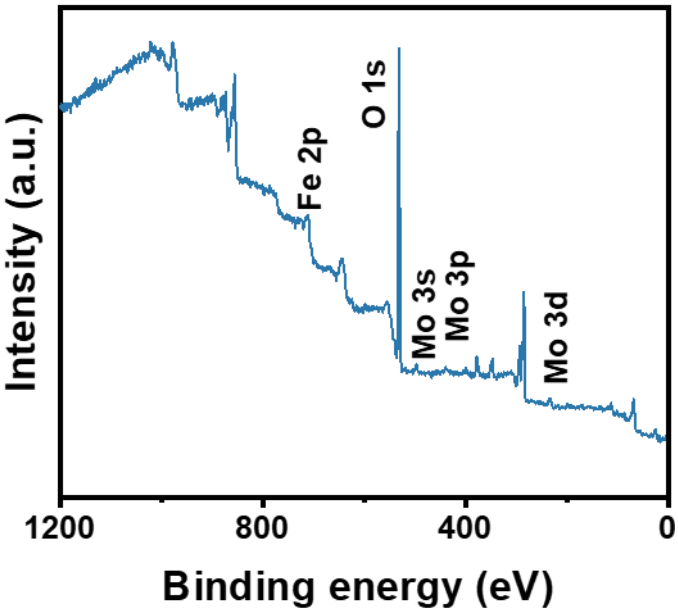

Fig. S5. XPS survey spectrum of FeMoOOH/NF-2h.

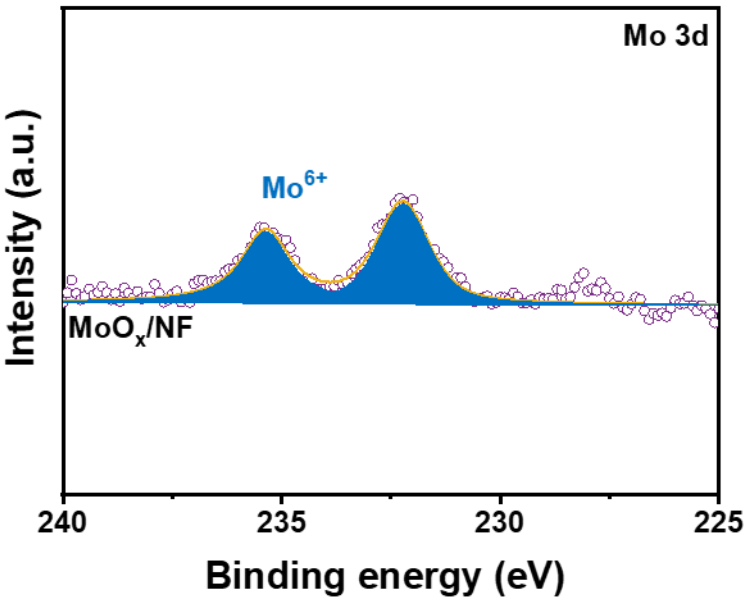

Fig. S6. XPS spectrum of Mo 3d in MoO_x/NF.

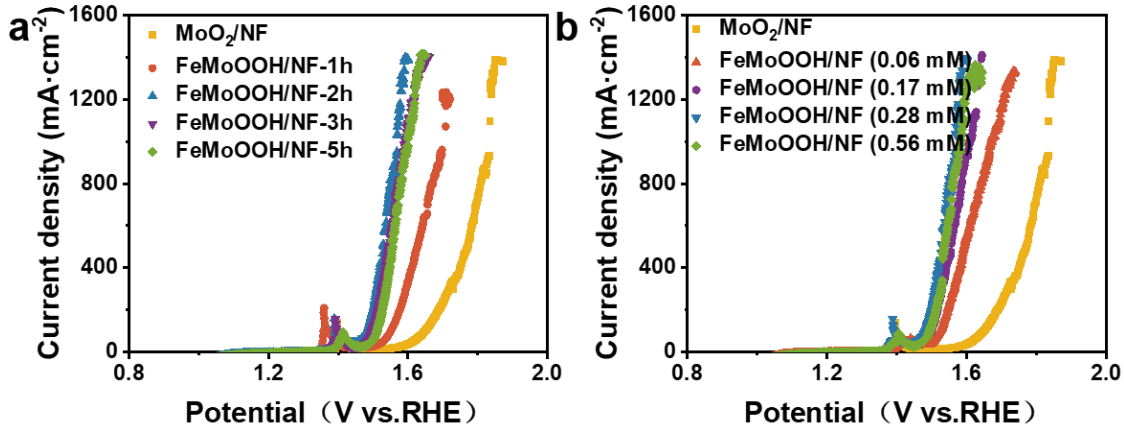

Fig. S7. Alkaline solution: (a) OER polarization curves of FeMoOOH/NF for different reconstruction time and (b) OER polarization curves for different electrolyte concentrations containing $Fe(NO_3)_3 \cdot 9H_2O$.

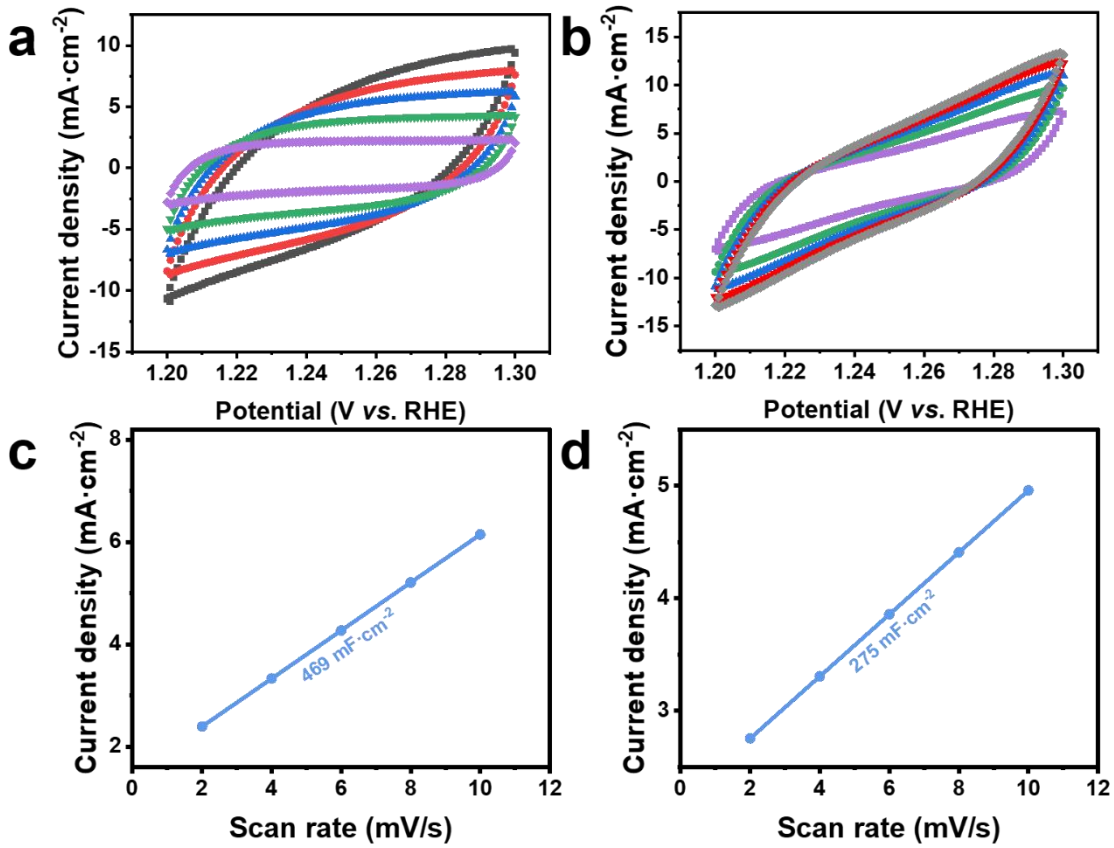

Fig. S8. Alkaline solution: CV curves of (a) FeMoOOH/NF and (b) MoO_x/NF. C_{dl} of (c) FeMoOOH/NF and (d) MoO_x/NF.

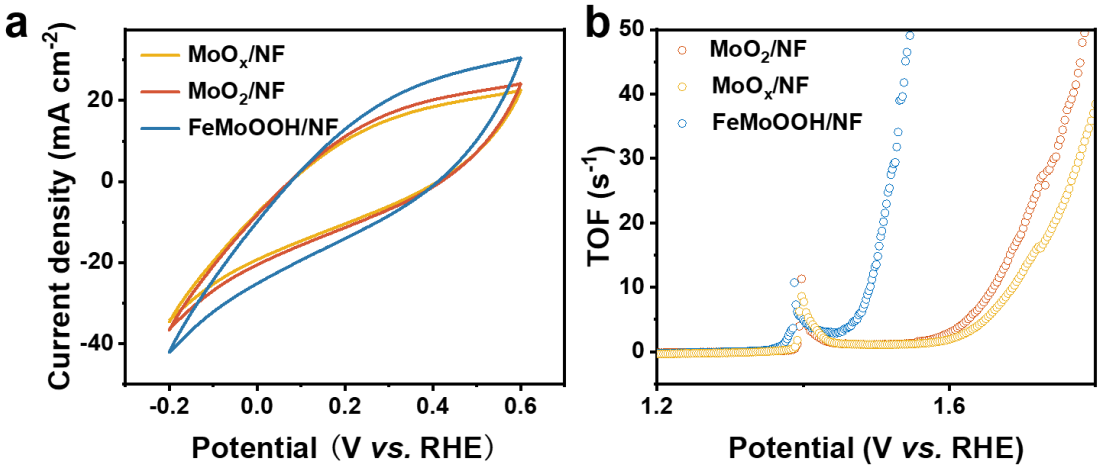

Fig. S9. (a) CVs for as-prepared samples in phosphate buffer (pH 7), (b) TOF.

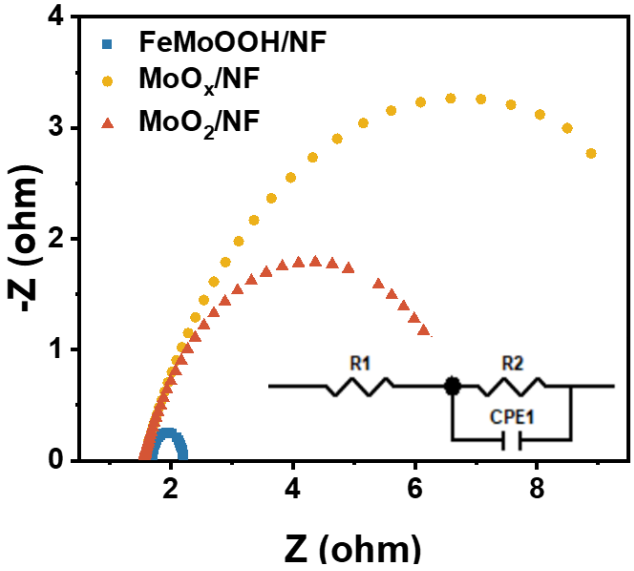

Fig. S10. Alkaline solution: EIS of FeMoOOH/NF, MoO_x/NF and MoO_2/NF.

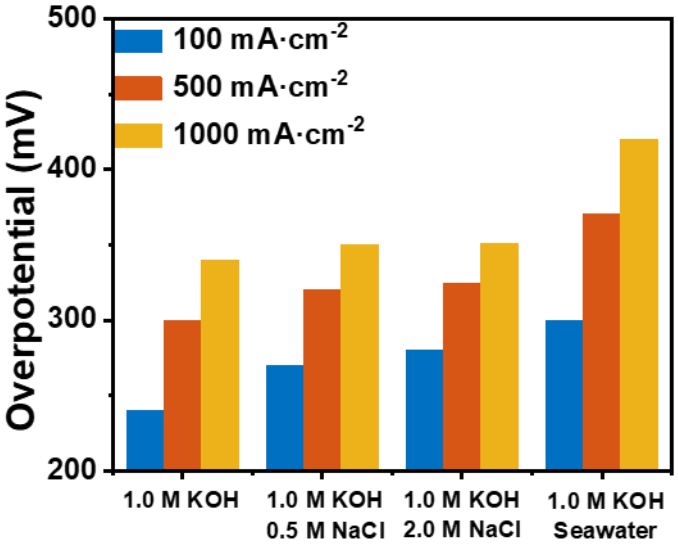

Fig. S11. Comparison of overpotential.

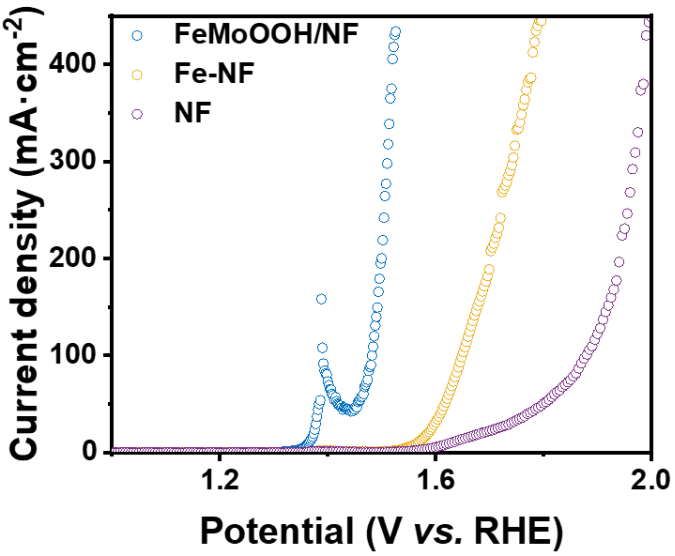

Fig. S12. LSV curves of FeMoOOH/NF, Fe-NF and NF.

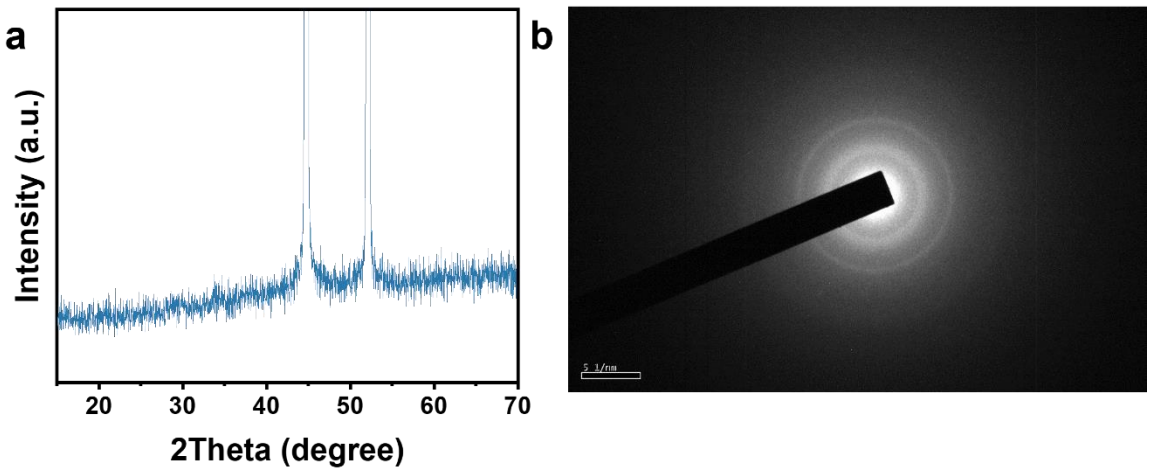

Fig. S13. (a) XRD of FeMoOOH/NF and (b) SAED of FeMoOOH/NF after the 100-hour I-t test.

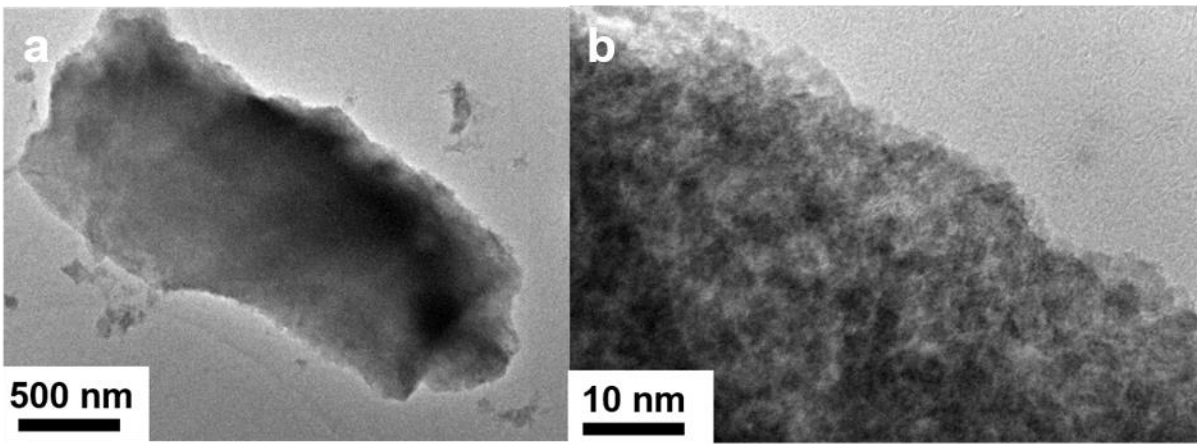

Fig. S14. TEM and HRTEM of FeMoOOH/NF after the 100-hour I-t test.

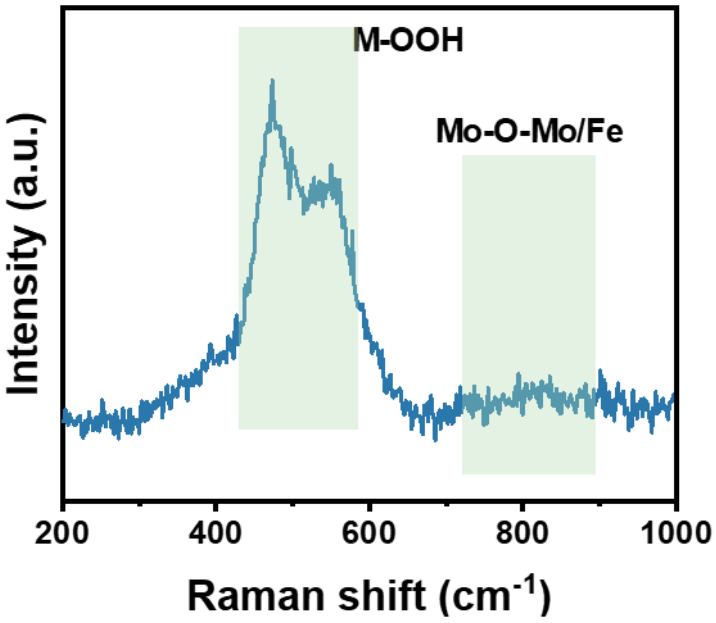

Fig. S15. Raman of FeMoOOH/NF after the 100-hour I-t test.

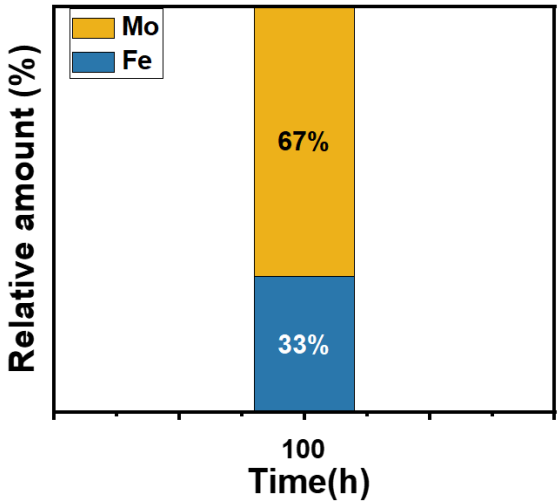

Fig. S16. ICP-MS tests of FeMoOOH/NF after the 100-hour I-t test.

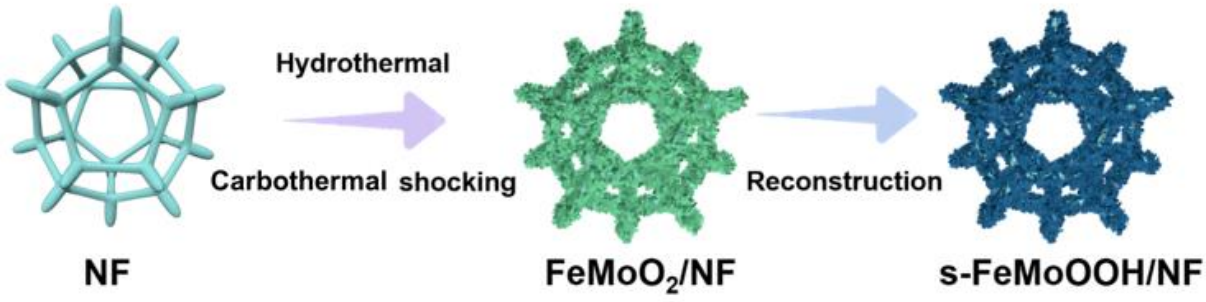

Fig. S17. Schematic diagram of the synthesis of surface amorphous FeMoOOH/NF (s-FeMoOOH/NF).

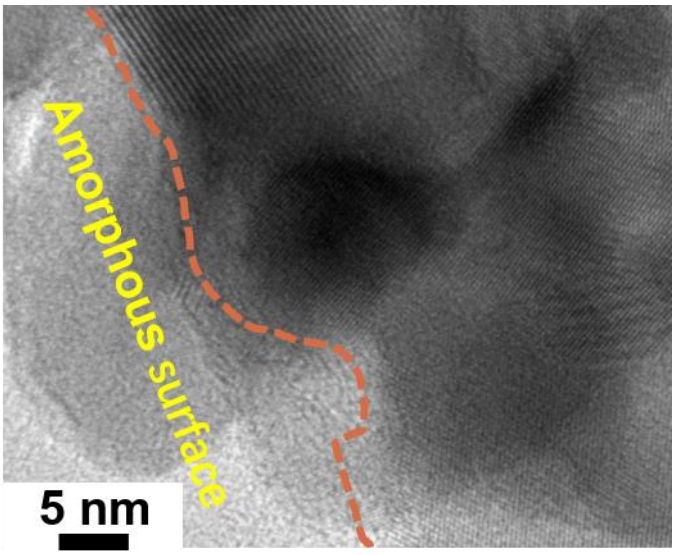

Fig. S18. TEM of s-FeMoOOH/NF.

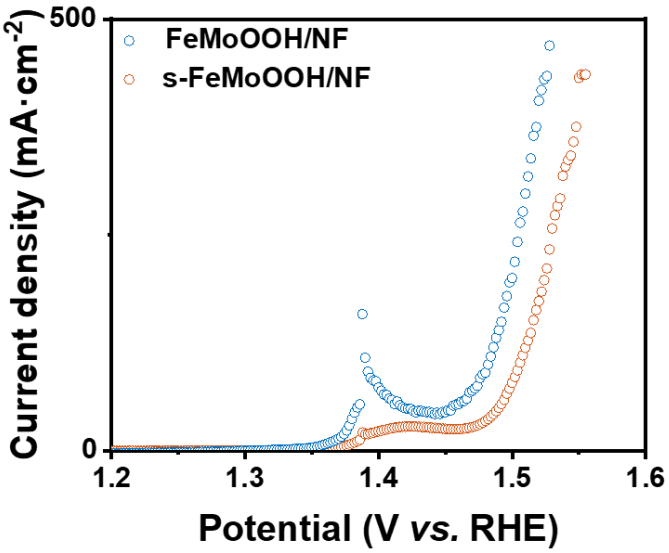

Fig. S19. LSV curves of alkaline solution.

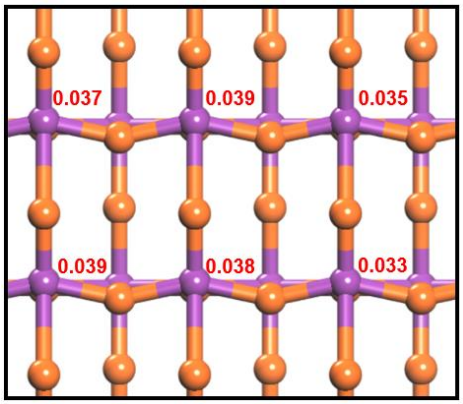

Fig. S20. Nucleophilic properties of atoms in MoO_x.

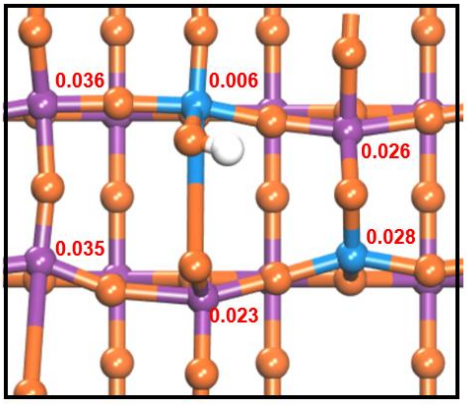

Fig. S21. Nucleophilic properties of atoms in FeMoOOH.

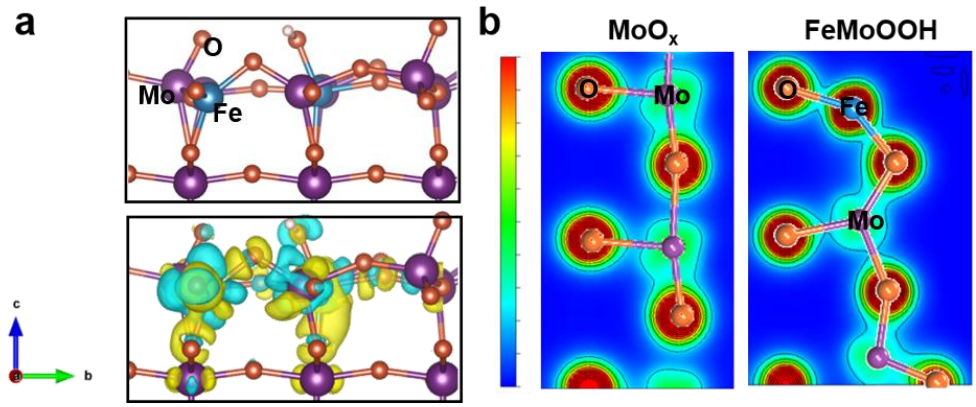

Fig. S22. Charge density difference plots.

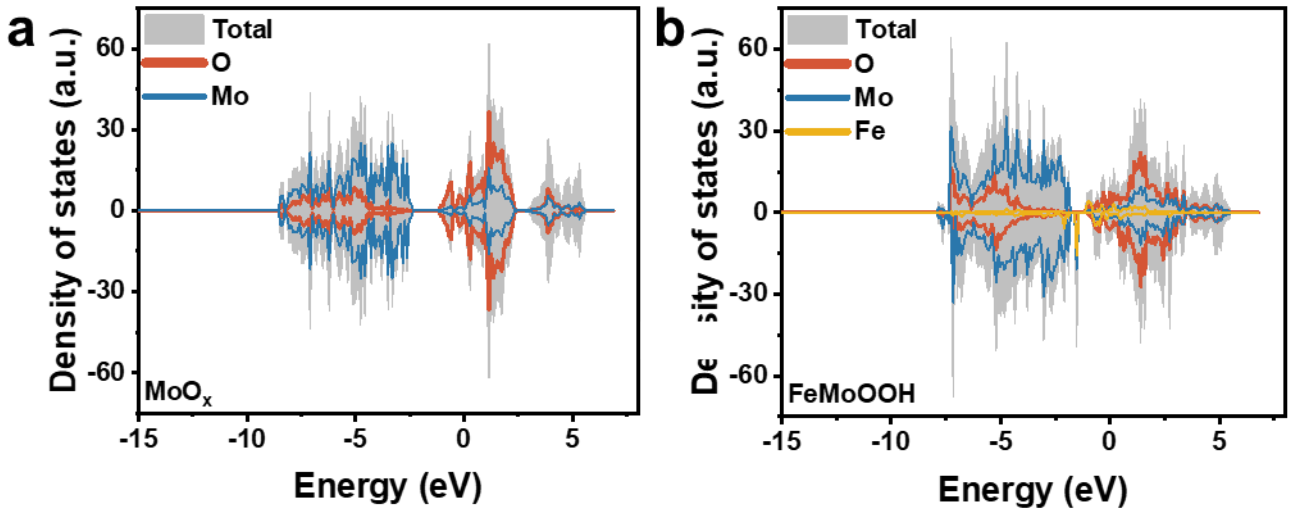

Fig. S23. DOS of (a) MoO_x and (b) FeMoOOH.

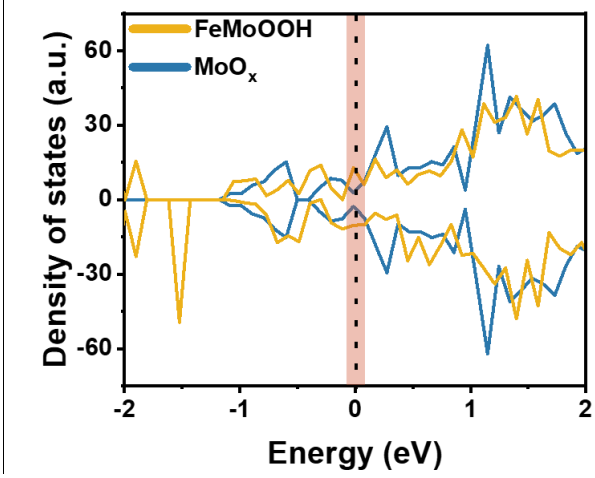

Fig. S24. TDOS of (a) MoO_x and (b) FeMoOOH.

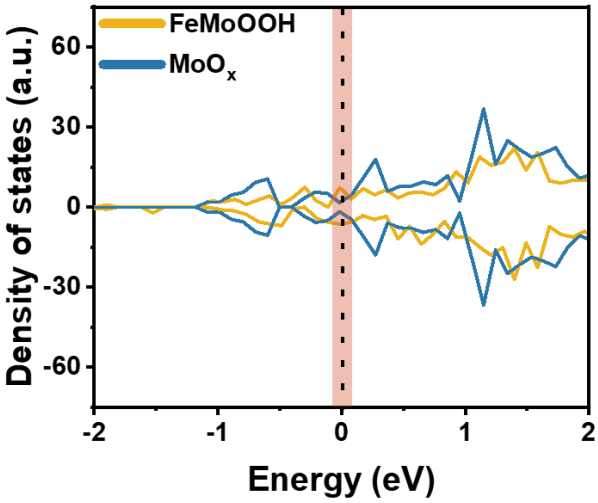

Fig. S25. p-band centers of MoO_x and FeMoOOH.

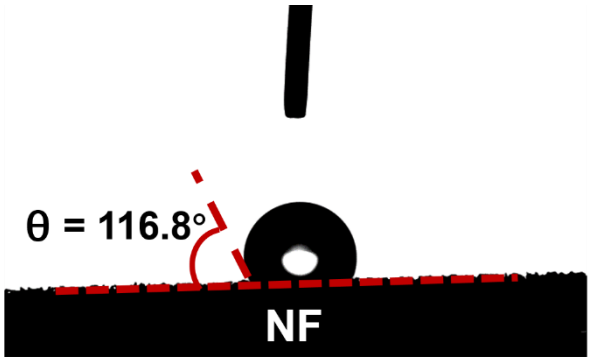

Fig. S26. Water droplets contact angle at NF.

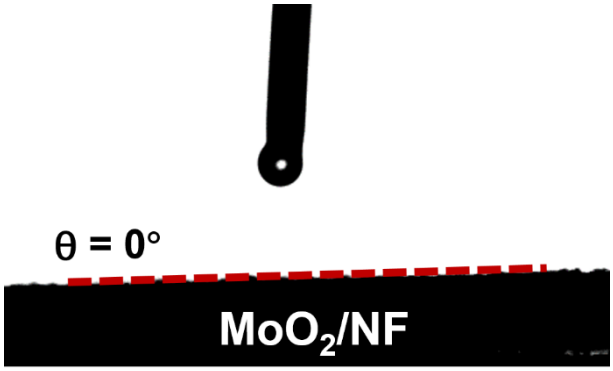

Fig. S27. Water droplets contact angle at MoO_2/NF.

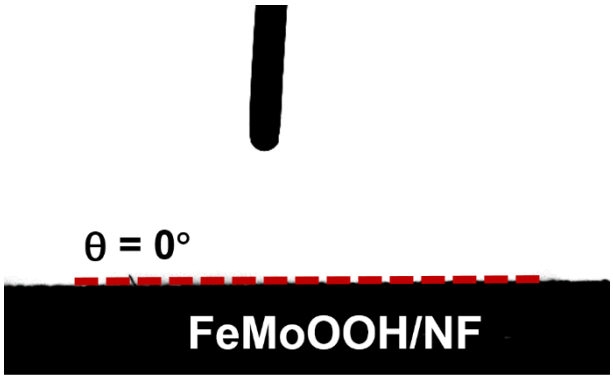

Fig. S28. Water droplets contact angle at FeMoOOH/NF.

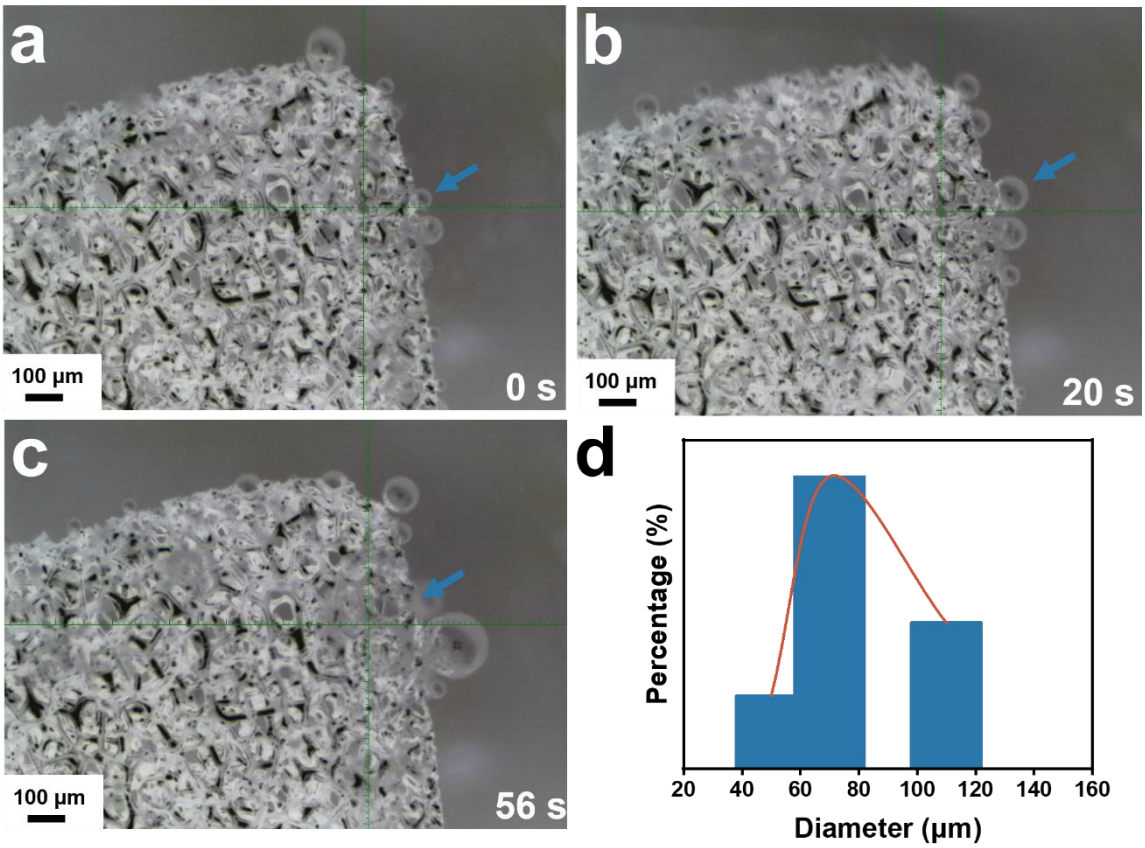

Fig. S29. Digital images showing the bubble generation behavior and the corresponding statistics of size distribution of releasing bubbles: (a-d) NF.

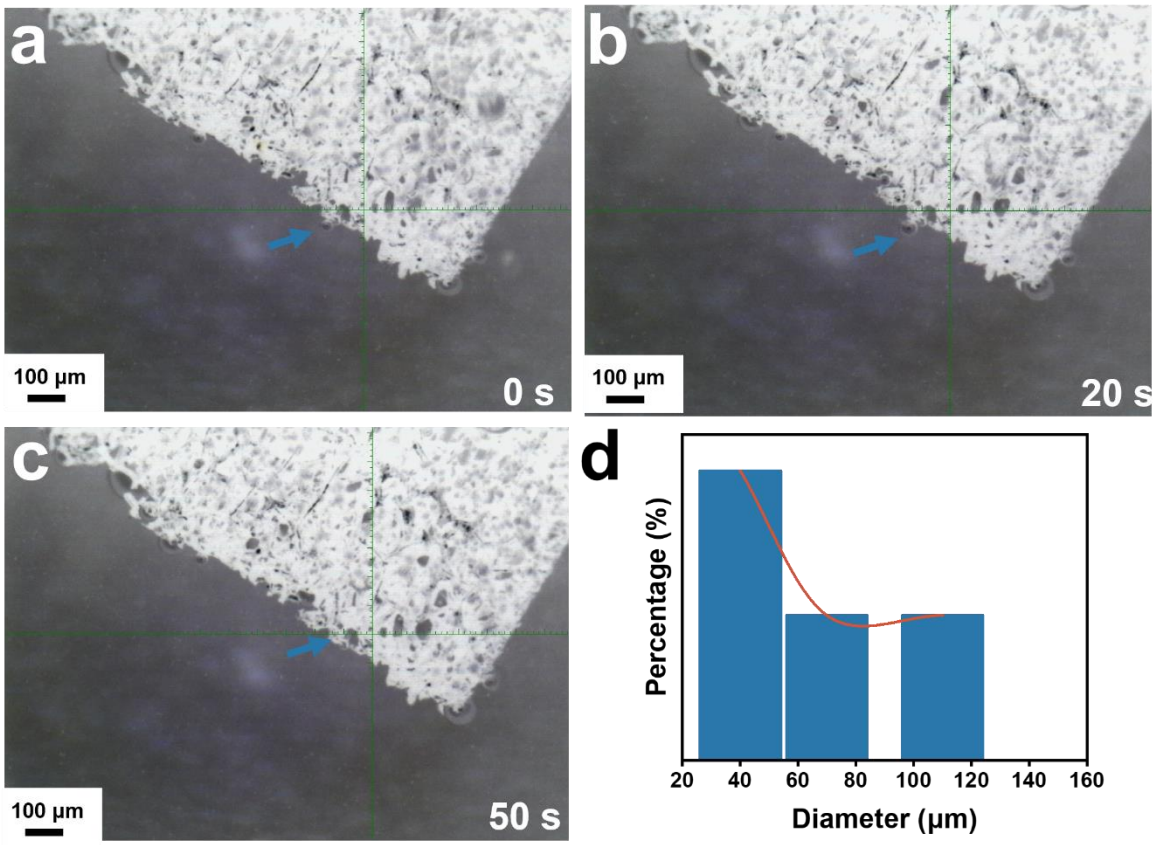

Fig. S30. Digital images showing the bubble generation behavior and the corresponding statistics of size distribution of releasing bubbles: (a-d) MoO_2/NF.

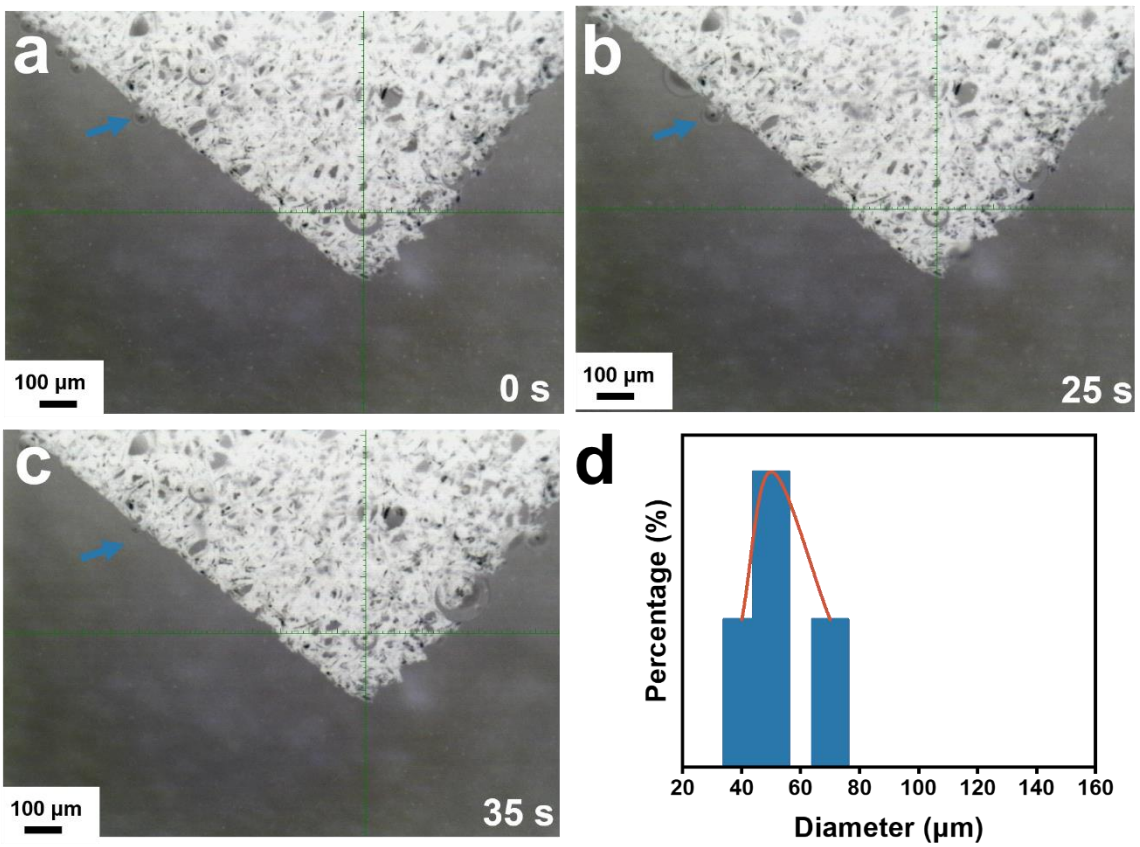

Fig. S31. Digital images showing the bubble generation behavior and the corresponding statistics of size distribution of releasing bubbles: (a-d) FeMoOOH/NF.

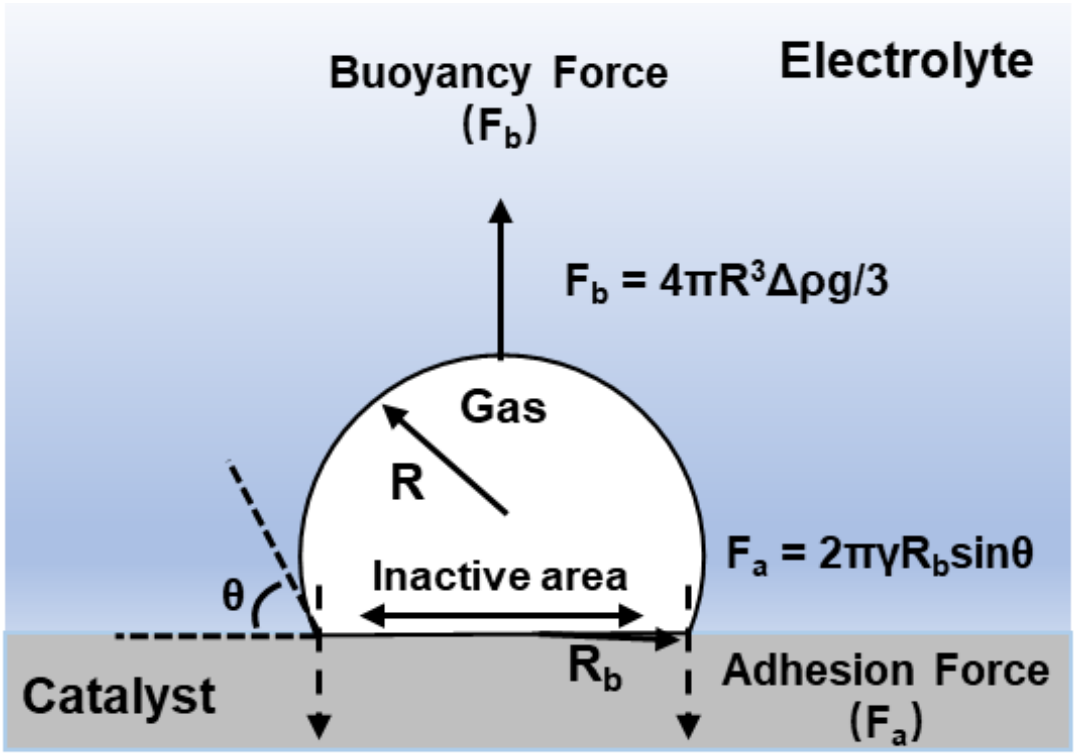

Fig. S32. The scheme for a mechanism of bubble-detachment.

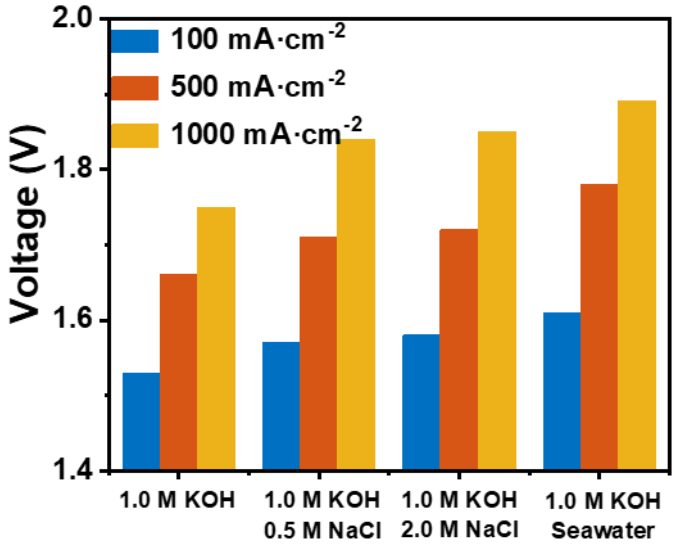

Fig. S33. Comparison of overpotential.

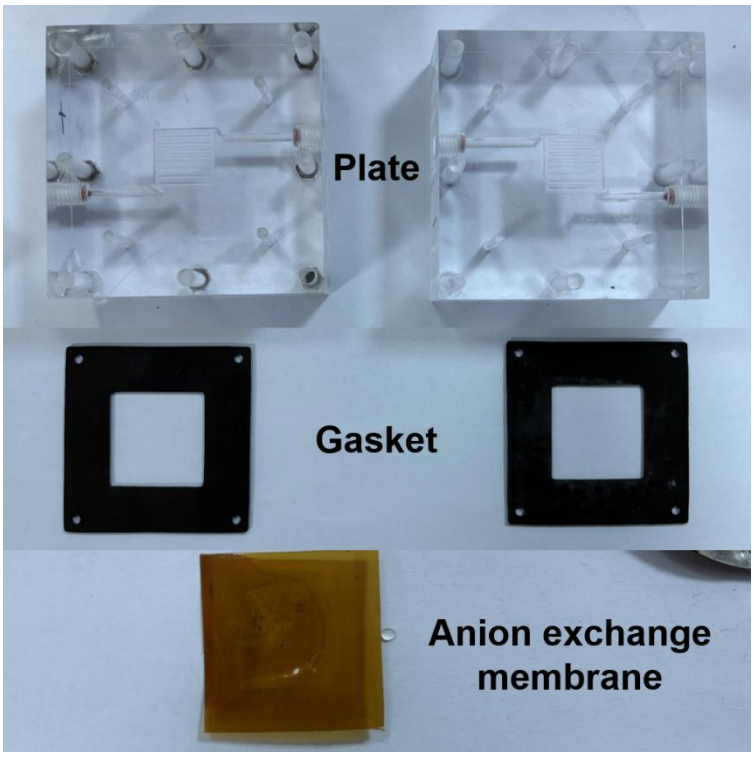

Fig. S34. Optical picture of AEM.

Tables

Table S1. OER performance of recently reported catalysts in 1 M KOH.

Catalysts	Electrolyte	η_{10} (mV)	η_{100} (mV)	Reference
FeMoOOH/NF	**1 M KOH**	**-**	**240**	***This work***
Ru SAs-MoO_{3-x}/NF	1 M KOH	-	282	*Adv. Sci. 2023, 10, 2300342*
Ir_1/Ni LDH-T	1 M KOH	228	-	*Nat. Commun. 2024, 15, 559*
LQNMP-Co_2O_3	1 M KOH	266	-	*ACS Nano 2024, 10.1021/acsnano.3c11199*
Fe-Ni-CoOOH-TPA	1 M KOH	236	-	*ACS Catal. 2024, 14, 1553–1566*
Co@Mo_2CT_x	1 M KOH	390	-	*Appl. Catal. B Environ. 346, 2024, 123731*
$NiV_{0.1}$-BLDH/NiCoP/NF	1 M KOH	-	268	*Adv. Funct. Mater.2024, 2315949*
V-$Co_2P_4O_{12}$/CC	1 M KOH	316	-	*Adv. Funct. Mater.2024, 2313974*
10.6 wt % Co SAC	1 M KOH	351	-	*J. Am. Chem. Soc. 2023, 145, 8052–8063*
$NiMoO_4$	1 M KOH	260	-	*Nano-Micro Lett. 2023, 15, 30*
Li-α-MoO_3/CFP	1 M KOH	458	-	*ACS Materials Lett. 2023, 5, 1196–1201*
FeCoPBA-VCN	1 M KOH	218	-	*Adv. Energy Mater. 2023, 2302403*
CoO/Co_3O_4/Ti	1 M KOH	270	-	*Angew. Chem. Int. Ed. 2020, 59,6929 –6935*
CoO/Co_3O_4/CC	1 M KOH	260	-	*Angew. Chem. Int. Ed.2020, 59,6929 –6935*
V_O-$CoMoO_4$@Cu_2S/CF	1 M KOH	181	320	*Chem. Eng. J. 477, 2023, 147016*
Ru@RuO_x/NCN	1 M KOH	270	-	*J. Energy Chem. 2023, 87, 286-294*
FeOOH/Ni_3S_2/NF	1 M KOH	-	268	*Small 2023, 2309371*

Co_3Mo/Mo_2C@NC	1 M KOH	282	355	*Adv. Funct. Mater.2024, 2314247*
MoS_2@Co	1 M KOH	370	-	*Energy Environ. Mater. 2024, 0, e12702*
$NiCo_2O_4$@CeO_2	1 M KOH	228	-	*Chem. Eng. J. 482, 2024, 148787*
Ni_3S_2/Fe_3O_4/NF	1 M KOH	220	-	*J. Colloid Interface Sci. 2024, 660, 440-448*

Table S2. OER performance of recently reported catalysts in 1 M KOH Seawater.

Catalysts	Electrolyte	η_{10} (mV)	η_{100} (mV)	Reference
FeMoOOH/NF	**1 M KOH Seawater**	**-**	**300**	***This work***
$Co_2Mo_3O_8/MoO_2$/NF	1 M KOH Seawater	-	320 (η_{40})	*Appl. Catal. B Environ. 338, 2023, 123015*
FeMoNi/NF	1 M KOH Seawater	-	~310	*Appl. Catal. B Environ. 340, 2024, 123277*
$(NiFeCoV)S_2$	1 M KOH Seawater	-	299	*J. Colloid Interface Sci. 2023, 645, 724–734.*
Ni_2P-Fe_2P/NF	1 M KOH Seawater	240	305	*Adv. Funct. Mater.2021, 31, 2006484.*
Fe-MoO_2/NF	1 M KOH Seawater	-	340	*Mater. Horiz., 2024, 10.1039/D3MH01757E*
CoSe/$MoSe_2$	1 M KOH Seawater	350	-	*ACS Sustain. Chem. Eng. 2022, 10, 30, 9980–9990*
NiTe@FeOOH	1 M KOH Seawater	-	280	*Chem. Eng. J. 2023, 474, 145568-145575*

Table S3. OWS performance of recently reported catalysts in alkaline water.

Catalysts	Electrolyte	η_{100} (V)	η_{1000} (V)	Reference
$Co_2Mo_3O_8$/MoO_2/NF // FeMoOOH/NF	**1 M KOH**	**1.53**	**1.75**	***This work***
R-CoC_2O_4@Mxene // R-CoC_2O_4@MXene	1 M KOH	~1.61 (η_{80})	-	*Nat. Commun. 2022, 13, 5785*
Fe-Ni_2Pv||Fe-Ni_2Pv	1 M KOH	-	1.86	*Adv. Mater. 2024, 36, 2307395*
V-$Co_2P_4O_{12}$/CC // V-$Co_2P_4O_{12}$/CC	1 M KOH	1.60 (η_{10})	-	*Adv. Funct. Mater. 2024, 2313974*
FMCO/NF // FMCO/NF	1 M KOH	~1.65 (η_{40})	-	*Appl. Catal. B Environ. 2023, 328, 122488*
CoFe-Ni_2P// CoFe-Ni_2P	1 M KOH	1.73	1.84 (η_{500})	*Adv. Energy Mater. 2023, 2301475*
Fe-P-CMO// Fe-P-CMO	1 M KOH	1.59	-	*Appl. Catal. B Environ. 2024, 346, 123741*
Ru SAs-MoO_{3-x}/NF // Ru SAs-MoO_{3-x}/NF	1 M KOH	1.71	-	*Adv. Sci. 2023, 10, 2300342*

Table S4. OWS performance of recently reported catalysts in alkaline seawater.

Catalysts	Electrolyte	η_{100} (V)	η_{1000} (V)	Reference
$Co_2Mo_3O_8$/MoO_2/NF/NF // FeMoOOH/NF	**1 M KOH Seawater**	**1.61**	**1.89**	***This work***
R-CoC_2O_4@Mxene // R-CoC_2O_4@MXene	1 M KOH Seawater	~1.70 (η_{80})	-	*Nat. Commun. 2022, 13, 5785*
CoFe-Ni_2P// CoFe-Ni_2P	1 M KOH Seawater	1.74	1.89 (η_{500})	*Adv. Energy Mater. 2023, 2301475*
Ru SAs-MoO_{3-x}/NF // Ru SAs-MoO_{3-x}/NF	1 M KOH Seawater	1.76		*Adv. Sci. 2023, 10, 2300342*
MoO_x/$Co(OH)_2$/NF // NiFe-LDH/NF	1 M KOH Seawater	1.74	-	*Nano Energy 2024, 121, 109246*
FeMoNi/NF // FeMoNi/NF	1 M KOH Seawater	~1.68	-	*Appl. Catal. B Environ. 2024, 340, 123277*
Mo–Ru/CNTs//RuO_2	1 M KOH Seawater	1.54 (η_{40})	-	*J. Mater. Chem. A, 2023,11, 22430-22440*
$Co_2Mo_3O_8$/MoO_2/NF // $Co_2Mo_3O_8$/MoO_2/NF	1 M KOH Seawater	~1.76	-	*Appl. Catal. B Environ. 2024, 338, 123015*
Pt2/$Ni(OH)_2$/NF // RuO_2/NF	1 M KOH Seawater	`1.80	-	*Appl. Catal. B Environ. 2023, 331, 122703*

Table S5. Solar-to-hydrogen (STH) conversion efficiency with different reported solar cell.

Catalysts	Solar cell	STH efficiency	Reference
$Co_2Mo_3O_8$/MoO_2/NF//FeMoOOH/NF	Perovskite solar cell	14.3	*This work*
	Triple-junction solar cell ($GaInP_2$/InGaAs/Ge)	~18.3	*Nat. Sustain. 2024, 7,158-167*
	Commercial GaAs solar cell	~19.6	*Carbon Energy, 2023, e217*
	Perovskite single-junction device stack glass/ITO/NiO_x/perovskite/C60/Au,	~21.3	*J. Mater. Chem. A, 2021,9, 14085-14092*

Table S6. Comparison between $Co_2Mo_3O_8/MoO_2$/NF//FeMoOOH/NF and other reported electrolysers of unit electricity consumption per cubic meter hydrogen (E_{H2}) and electricity-to-hydrogen energy conversion efficiency (η_{ETH}).

Electrolyser	E_{H2} (kW h m^{-3})	η_{ETH} (%)	Reference
$Co_2Mo_3O_8/MoO_2$/NF//FeMoOOH/NF (1 M KOH Seawater)	**4.04**	**87.6**	***This work***
$Co_2Mo_3O_8/MoO_2$/NF//FeMoOOH/NF (1 M KOH)	**3.94**	**89.7**	***This work***
NMFSOH	3.99	88.7	*Adv. Energy Mater. 2023, 13, 2301222*
Fe (FeNiMo)O_2 /NF	3.97	89.1	*Small, 2024, 20, 2404786*
NiFe LDH||NiFe LDH	4.49	78.8	*Small, 2022, 18, e2104354*
NiFe LDH-PMo||NiFe LDH-PMo	4.44	79.2	*Adv Mater, 2022, 34, e2110696*
NiFe||NiFe	4.06	88.1	*Energ. Environ. Sci., 2020, 13, 86-95.*
NiMoO/NiMoS||NiMoO/NiMoS	4.21	84.0	*Nat Commun, 2020, 11, 5462-5474*
CoMoS||CoMoS	4.52	78.2	*Angew. Chem. Int. Ed., 2020, 59, 1659-1665.*
NiFeMoO||NiFeMoO	6.28	56.3	*Adv Sci, 2020, 7, 1902034.*

Table S7. Price of the scaling-up prepared FeMoOOH/NF catalyst.

Material	Suppliers	Price (US$ kg^{-1})	Component price in catalyst (US$ m^{-2})	Total price of catalyst (US$ m^{-2})
$(NH_4)_6Mo_7O_{24}{\cdot}4H_2O$	Shanghai Aladdin Biochemical Technology Co., Ltd	80.8	37.0	84.2
$Fe(NO_3)_3{\cdot}6H_2O$	Shanghai Aladdin Biochemical Technology Co., Ltd	47.5	17.2	
Ni foam	Kunshan Guangjiayuan Technology Co., Ltd	-	~30	

Table S8. Price of the scaling-up prepared FeMoOOH/NF.

Catalysts	Support	Suppliers	Price per 1 m^2 catalyst (US$ m^{-2})
FeMoOOH/NF	Ni foam	**This work**	84.27
Raney Ni	Ni foam	Jiangsu Leini Metal Tech. Co., Ltd	60
Pt black	Carbon cloth	Fuel Cell store	9100